archives
of thermodynamics
Vol. **42**(2021), No. 4, 3–15
DOI: 10.24425/ather.2021.137560

Selection of a numerical model to predict the flow in a fan with a cycloidal rotor

TOMASZ STAŚKO*
MIROSŁAW MAJKUT
SŁAWOMIR DYKAS
KRYSTIAN SMOŁKA

Department of Power Engineering and Turbomachinery, Silesian University of Technology, Konarskiego 18, 44-100 Gliwice, Poland

Abstract A fan with a cycloidal rotor (CRF) is a promising design for application in HVAC (heat, ventilation and air conditioning) systems. Despite the widespread use of the CRF design as a form of propulsion, there are practically no scientific publications examining the possibility of using it as the HVAC fan. The choice of the cycloidal rotor facilitates the operating procedure and widens the range of operating conditions. The paper focuses on the use of the CRF in HVAC, especially as a blowing machine integrated with rectangular ducts, presenting, and discussing the search for the most efficient numerical model. The way of discretizing the computational domain, the turbulence models and the time integration method were tested. A four-blade open rotor fan with a cycloidal impeller was used both in the numerical and in the experimental model. The 2D and 3D CRF models created in the Ansys CFX package were adopted. After a mesh-independence study, different turbulence models were tested for the selected mesh. In the case of the 2D model, various turbulence models such as the SST and the RNG k-ε options were tested and compared with each other. The computational fluid dynamics simulations were compared with in-house experimental results of the velocity field measurements performed by means of laser Doppler anemometry and thermoanemometry. It turned out that the considered numerical models did not reflect the experimental measurements quantitatively. This may be due to the small differences in the shapes of the cycloids of the rotor blades in the numerical model and in real geometry.

Keywords: Fan; CFD; Cyclorotor

*Corresponding Author. Email: tomasz.stasko@polsl.pl

1 Introduction

The idea of the cycloidal rotor is mostly met in propulsion systems of MAVs (micro air vehicles). In this field, a mention should be made of the European CROP (Cycloidal Rotor Optimized for Propulsion) project from 2015, which aimed to create a "radically different propulsion system for aerial vehicles" [1–3]. The authors demonstrated the possibility of creating a new propulsion system based on a cycloidal device called the PECyT (plasma enhanced cycloidal thruster) [4]. The CROP has demonstrated that it is possible to combine the benefits of high flow instability with plasma-based boundary layer control [5–7]. Benedict and others [8–12] conducted a series of numerical and experimental studies on the cyclocopter. The focus was on the study of phenomena occurring during the cyclocopter flight and hovering [13–15]. The structure was modernized and its various variants were analysed as actual models were created [16]. The latest achievement in the field of propulsion is the Aria project [17], which resulted in the construction of a fully flying model. The results of the study highlighted the limitation of the flight electric endurance due to poor battery performance, as well as the need for reliable, lightweight equipment for such applications. The cycloidal rotor fan (CRF) is also used for ship propulsion in the form of a cycloidal propeller [18–20]. Due to the fact that it is a well-known design, scientific research focuses on improving the dynamics of the propeller and optimizing its operation by adjusting the control systems to current conditions. The idea of the cycloidal propeller also appears as an auxiliary propulsion system for ships. The cycloidal gearbox is also used to increase the efficiency of Darrieus wind turbines [21].

A novel approach to the cycloidal rotor is the idea of using it as a tidal machine to produce energy [22, 23]. This design uses a cycloidal rotor that is half-submerged in water. The aim of the research is to create a fully functional machine, which is to be cost-competitive with known renewable energy sources such as wind. The decision to verify the CRF application for power engineering and heat, ventilation and air conditioning (HVAC) systems was prompted by the fact that there are practically no scientific publications examining the possibility of using the device in this particular concept.

The CRF analysed herein belongs to the family of radial fans without a diffusor, and therefore it is called an open rotor fan. This concept is based on a system of rotating blades where the axis of rotation is parallel to the blade span [24–26]. The blade pitch angle is controlled by an independent

mechanical system. Thanks to such a design solution, each blade operates under similar conditions, so the blades are easier to optimize in terms of aerodynamic efficiency [27].

This paper presents an unsteady computational fluid dynamics (CFD) analysis of the impact of the pitch angle of the CFR blades in the flow through a rectangular duct. To make it possible, a special script was developed in the Ansys CFX Expression Language (CEL) [28].

In the experimental research on the velocity field measurement, the laser Doppler anemometry (LDA) and the thermoanemometry (TA) techniques were used. LDA is a contactless measurement method that does not disturb the measured velocity field. What is more, it does not require calibration because the parameters it depends on do not change due to external factors and are based on physico-optical parameters. The aim of the research is to check the possibility of using previous numerical models and examine the influence of the cycloidal function describing the movement of the blades on the fan overall performance.

2 Subject of investigation

The analysed radial fan with a cycloidal rotor consisted of four blades of the asymmetrical Clark Y profile with chord $c = 50$ mm. This airfoil is commonly used in aircraft designs due mainly to its capacity for lift force generation. The rotor full radius is $R = 70$ mm and the initial position of the blade angles is as follows: $\psi = 0$, $\pi/2$, π, and 1.5π (cf. Fig. 1).

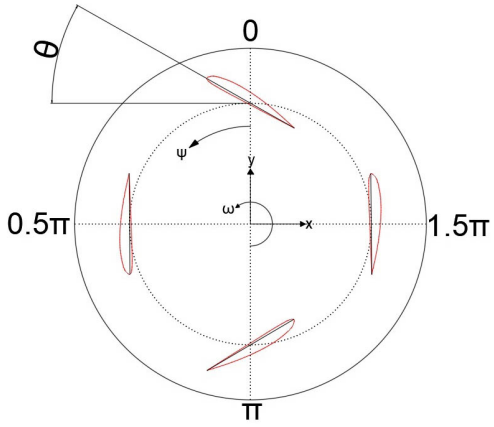

Figure 1: Configuration of the CRF.

Figure 1 shows the CRF inside the channel. The upper blade ($\psi = 0$) has a positive angle of incidence, while the opposite blade ($\psi = \pi$) has a negative angle. In addition, the other two blades ($\psi = \pi/2$ and $\psi = 1.5\pi$) in this state reach an incidence angle of 0°. This arrangement of the blades allows the flow to be generated through the rotor (from 'top' to 'bottom'). Each blade rotates around a point on the camber line in the middle of the chord [24, 29].

In cyclorotors, the pitch angle (θ) of the blades is adjusted by mechanical transmission. A four-point linkage system was used in the analysed machine due to its simple structure (Fig. 2) [24, 29].

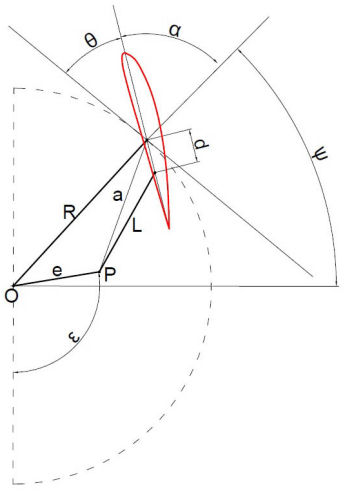

Figure 2: Schematic drawing showing geometrical parameters of the cyclorotor blade linkage configuration.

The first step was to determine the cycloidal function to properly adjust the fan blades. In order to visualize the changes in the optimization parameters of the blade angles, a program was written that enables appropriate application of the equations used in the process of numerical calculations, along with the geometric settings of the structure used in experimental tests [3, 8].

Depending on the input data (Fig. 2), the program solved the following equations

$$\alpha_1 = \sin^{-1}\left[\frac{e\cos\left(\psi + \varepsilon + \frac{\pi}{2}\right)}{a}\right], \tag{1}$$

$$a = \sqrt{e^2 + R^2 - 2eR\cos\left(\psi + \varepsilon + \frac{\pi}{2}\right)}, \tag{2}$$

$$L = \sqrt{a^2 + d^2 - 2ad\cos(\alpha_2)}. \tag{3}$$

The relationship between the position of the blade on the circle (ψ) and the angle of its deflection (θ) is expressed as

$$\theta = \frac{\pi}{2} - \sin^{-1}\left[\frac{e}{a}\cos(\psi + \varepsilon)\right] - \cos^{-1}\left[\frac{a^2 + d^2 - L^2}{2ad}\right]. \tag{4}$$

Based on the presented functions, an ideal cycloid was determined, being an inverse cosine function shifted by a certain angle (28° in the case under analysis). The predicted function for the model of the experimental stand was also determined using Eqs. (1)–(4). After making, assembling and calibrating the test rig for the chosen case, the actual cycloidal function for the given angles was obtained [3, 8, 30].

Figure 3 shows a comparison of 3 cycloids for the blade deflection angles θ depending on their position on the circle (circumference of the rotor). Cycloid 1 is the aforementioned cyclic function for an ideal cycloidal rotor. Cycloid 2 describes the predicted range of the deflection of the blades. Based on it, appropriate shifts of the mechanical adjustment were selected for a given angle. Cycloid 3 is the actual change in the angles of the blades measured on the experimental test stand. In principle, it can be assumed

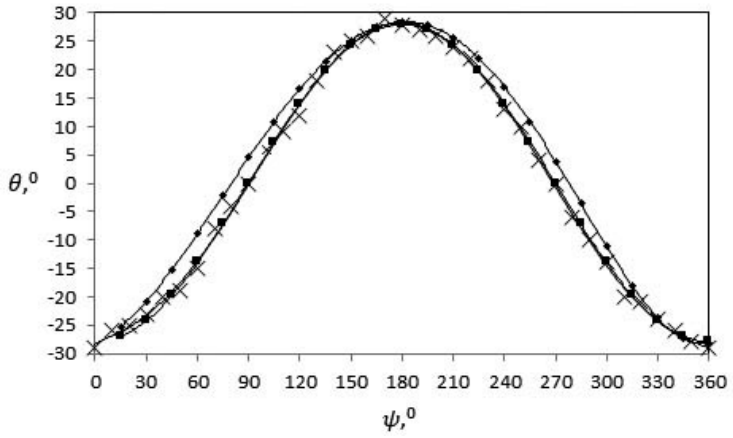

Figure 3: Comparison of cycloidal functions (Cycloid 1 – perfect cycloidal function, Cycloid 2 – predicted cycloidal function, Cycloid 3 – actual cycloidal function).

that the 3 cycloids under consideration converge to a satisfactory degree, and it can be concluded that the position control was performed correctly. The small differences between the angles (in most cases of less than 2–5°) may result from imperfections in the production of the CRF elements and their subsequent assembly, and from the occurrence of small assembly clearances.

The measurements were carried out using a thermoanemometric probe (TA) and an LDA system (Fig. 4). Experimental investigations were performed under the same conditions. The rotor angles were changed according to the Cycloid 3 shown in Fig. 3 at 1000 rpm. The measurements were carried out on 4 planes of the tunnel cross-section: at the inlet ($2R$ from the rotor centre) and at the outlet ($2R$, $4R$, and $6R$) (Fig. 4).

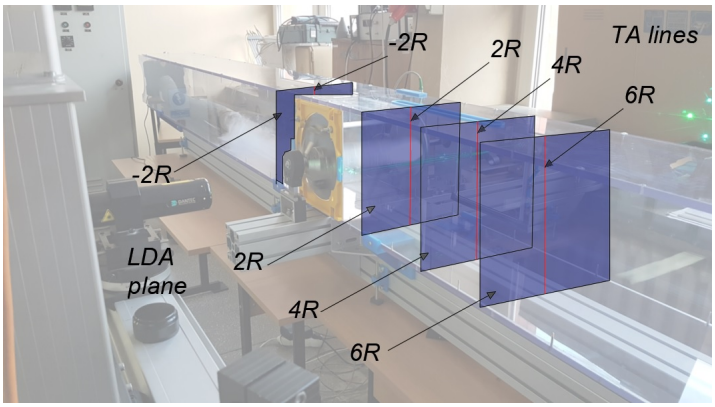

Figure 4: Measurement sections.

The LDA measurements were carried out on 4 planes (marked in dark blue). For each plane, a mesh of 180 points was created, which defined the places of laser measurement. For each point on the mesh, 500 measurements were made, the final value of which was the average value. The thermoanemometric probe measured the velocity profile in a line in the centre of the tunnel. For each plane, the measurement was started from the bottom of the tunnel shifting upwards by 1 cm. The probe measurement points coincided with those of the laser, and the same was done for 500 measurements at a point in 60 s. The experimental results in the form of velocity profiles for the cross-section are presented below (Fig. 5)

It can be seen that the results of the LDA and the TA measurements practically coincide, so the LDA measurement can be adopted as the reference measurement, as it does not interfere with the flow and is more ac-

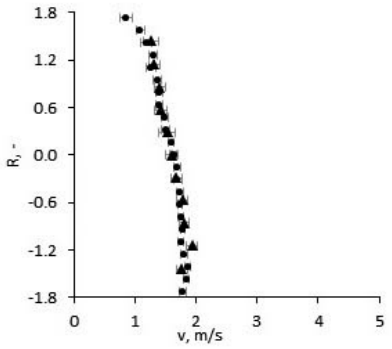

(a) Velocity profile in the inlet channel cross-section ($-2R$)

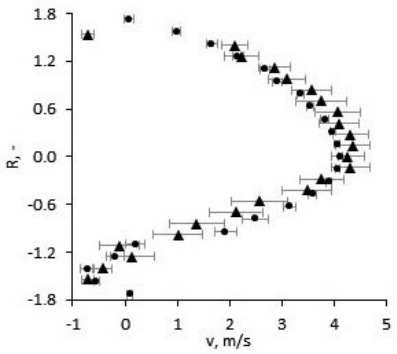

(b) Velocity profile in the outlet channel cross-section ($2R$)

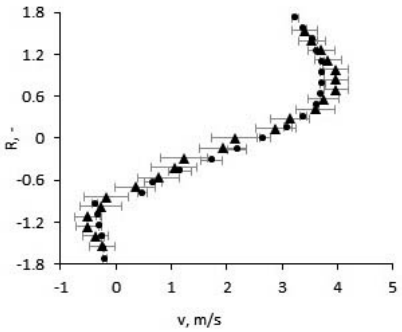

(c) Velocity profile in the outlet channel cross-section ($4R$)

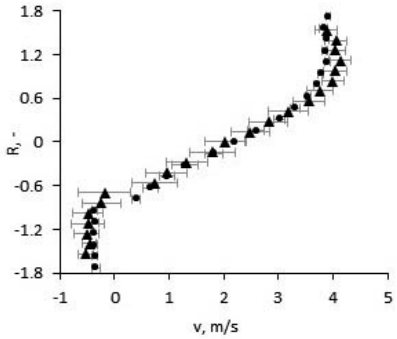

(d) Velocity profile in the outlet channel cross-section ($6R$)

Figure 5: Comparison of the velocity profiles measured experimentally. Velocity profiles measured: (a) at the inlet at $2R$, (b) at the outlet at $2R$, (c) at the outlet at $4R$, (d) at the outlet at $6R$.

curate compared to the thermoanemometric probe. The graphs also shows the standard deviation. Its high value is due to the formation of significant turbulence in the flow. The measurement accuracy will be improved in the future by increasing the measurement time and the number of recorded samples.

The analysis was conducted using a mesh from our previous works [26, 27], where a mesh-independent-solution study was performed. The numerical model of the cycloidal rotor fan consisted essentially of 6 domains: a rectangular tunnel (not rotating), a rotating domain (with 1000rpm) with four

holes for rotors and one hole for a shaft, and four domains with a blade. For the interface between the domains the general connection was used, with an in-house script for the stator-rotor interaction. The refinement of the blade mesh was adjusted by changing the number of elements on the outer and inner edges of the mesh model. Similarly, the density of the inner domain and of the tunnel was set in the same way. The blade mesh in one XY-plane consisted of about 13k elements, the blade inner edge had inflation on it. The boundary layer was introduced to ensure $y^+ = 1$, where y^+ is a dimensionless number based on the distance to the wall. The rotating domain consisted of about 10^4 elements and the tunnel had about 32k. Because unsteady simulations take a lot of time, it was decided to use the 2D model only. The boundary conditions at the inlet were as follows: total absolute pressure of 1 bar and total absolute temperature of 20°C. At the outlet, the outer boundary conditions with static pressure of 1 bar was adopted. The inlet turbulence intensity was set to mid value, according to the Ansys CFX settings. This corresponds to the conditions during the experiment.

The schematic drawing of the model and the mesh parameters are presented below in Fig. 6. Based on the described mesh, for Cycloid 1 the

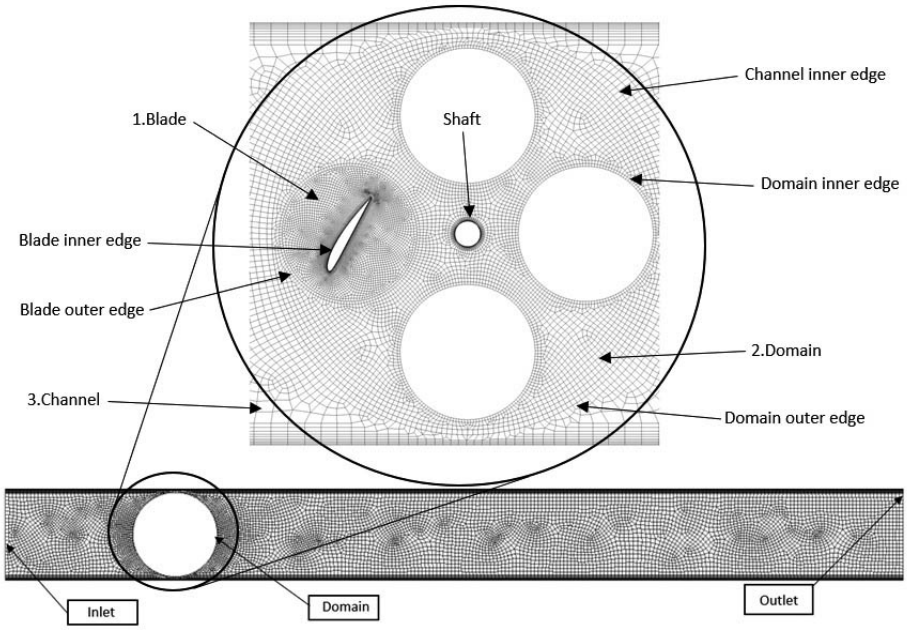

Figure 6: Schematic representation of the numerical model elements.

following turbulence models were tested: SST, k-ω and RNG k-ε. It was assumed that slight differences in angles would not affect the operation of the rotor significantly.

A comparison of computational results with the results obtained from the LDA experiment is presented in Fig. 7. As it can be seen from the results gathered above, it is very difficult to clearly determine which turbulence model is the best. For the inlet profile (Fig. 7a), the k-ω model is the closest to the measured values, but the shape of the velocity profile is generally similar for all models. On the other hand, in numerical models

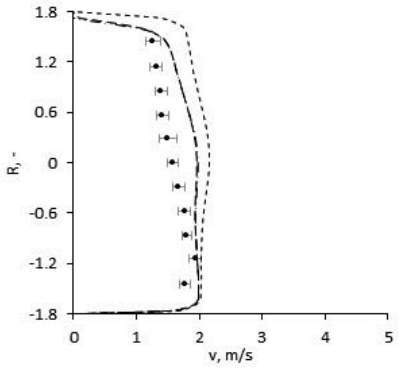

(a) Velocity profile in the inlet channel cross-section ($-2R$)

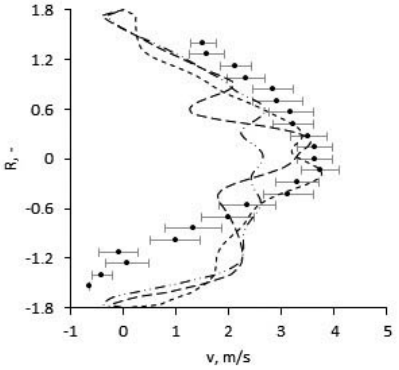

(b) Velocity profile in the outlet channel cross-section ($2R$)

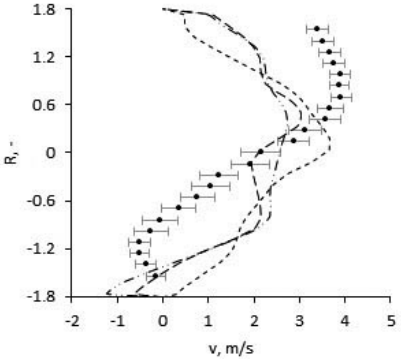

(c) Velocity profile in the outlet channel cross-section ($4R$)

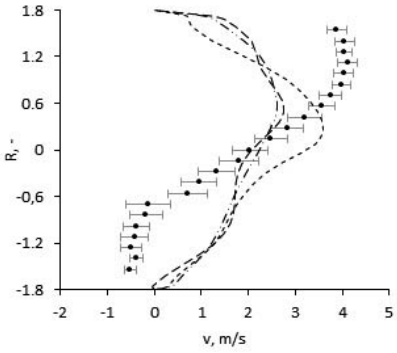

(d) Velocity profile in the outlet channel cross-section ($6R$)

Figure 7: Comparison of the velocity profiles across the LDA with different numerical turbulence models. Velocity profiles measured: (a) at the inlet at $2R$, (b) at the outlet at $2R$, (c) at the outlet at $4R$, (d) at the outlet at $6R$.

in the outlet profile $2R$, the formation of characteristic 'peaks' in the flow can be noticed. These peaks are the effect of the backward influence of the blade. Additionally, a velocity drops in the lower part of the tunnel bigger than in reality and formation of areas with a negative velocity value can be observed. Due to the complexity of the phenomena occurring in this cross-section, such as the aforementioned impact of the rotor or the process of vortex formation, it may turn out that it is impossible to perfectly reproduce the conditions in the numerical model. Based on the other measurements, it can be seen that the flow is actually directed more towards the top of the channel, whereas in the numerical model it moves closer to the centre.

3 Summary and conclusions

The ideal function describing the movement of the blade in the cycloidal rotor was determined for a given maximum deflection angle θ. Then, appropriate parameters of the mechanical adjustment were selected. After the assembly and after the measurement of the actual quantities characterizing the CRF, the predicted function describing the movement of the blade was determined. After proper calibration and setting of the CRF blades, the deflection angle (θ) of the blades was measured and a true cycloidal function was obtained. Experimental measurements were also made using two different methods: the Laser Doppler Anemometry technique and a thermoanemometric probe. A numerical model of a CRF closed in a channel was created to compare the experimental results with the numerical ones. The experience gained from previous studies was used and extended to select the optimal turbulence model.

The following conclusions were reached:

- Based on the described model and the created program in the CFX, it can be concluded that the course of the real cycloid function determining the change of the CRF blade angles on the stand is determined and implemented correctly, satisfactorily coinciding with the ideal course of this function.
- The two different measurement methods: LDA and TA are in agreement. Thanks to this, it is possible to use one of them as a reference measurement method in current and future research. Our future experimental research will deal with measurements for different flow conditions.

- The use of previously applied meshes and the model simplification did not give satisfactory results. It is likely that even slight changes in the course and implementation of the cycloidal function by the CRF may lead to significant changes in the flow. In the future, it is recommended that numerical calculations are performed based on the real cycloid function.
- It also seems that despite relatively low velocities at the inlet profile and a relatively stable flow, the mesh should be finer at that point. This would also apply to the entire outlet profile under analysis – from $2R$ to $6R$.
- Among the analysed models, the closest in terms of the shape and adjustment of the velocity profile, and the average velocity values is the RNG k-ε turbulence model. The authors intend to conduct calculations using this model in the future.

Future research will be focused on the search of a CFD model being a compromise between accuracy and time of the calculations and suitable for the purpose of the CRF optimization.

Acknowledgement The presented results were performed within the Statutory Research Funds of the Silesian University of Technology.

Received 7 June 2021

References

[1] Morandini M., Xisto C., Pascoa J., Quaranta G., Gagnon L., Masarati P.: *Aeroelastic analysis of a cycloidal rotor under various operating conditions*. J. Aircraft. **55**(2018), 4, 1675–1688.

[2] Muscarello V., Masarati P., Quaranta G., Georges T., Gomand J., Malburet F., Marilena P.: *Instability mechanism of roll/lateral biodynamic rotorcraft–pilot couplings*. J. Am. Helicopter Soc. **63**(2018), 1–13.

[3] Xisto C. Leger J., Pascoa J., Gagnon L., Masarati P., Angeli D., Dumas A.: *Parametric analysis of a large-scale cycloidal rotor in hovering conditions*. J. Aerospace Eng. **30**(2017), 1.

[4] Xisto C., Pascoa J., Abdollahzadeh M., Leger J., Masarati P., Gagnon L., Schwaiger M., Wills D.: *PECyT – plasma enhanced cycloidal thruster*. In: Proc. 50th AIAA/ASME/SAE/ASEE Joint Propulsion Conf. July 28–30, 2014, Cleveland.

[5] Andrisani A., Angeli D., Dumas A.: *Optimal pitching schedules for a cycloidal rotor in hovering*. Aircr. Eng. Aerosp. Tec. **88**(2016), 5.

[6] Xisto C., Pascoa J., Leger J.: *Cycloidal rotor propulsion system with plasma enhanced aerodynamics*. In: Proc. ASME 2014 Int.l Mechanical Engineering Congress and Exposition; Montreal, Nov. 14–20, 2014; V001T01A005.

[7] Xisto C., Pascoa J., Trancossi M.: *Geometrical parameters influencing the aerodynamic efficiency of a small-scale self-pitch high solidity VAWT*. J. Sol. Energy Eng. **138**(2016), 031006.

[8] Benedict M.: *Fundamental understanding of cycloidal-rotor concept for micro air vehicle applications*. PhD thesis, Univ. Maryland, College Park, 2010.

[9] Benedict M., Ramasamy M., Chopra I.: *Improving the aerodynamic performance of micro-air-vehicle-scale cycloidal rotor: An experimental approach*. J. Aircraft 47(20104), 1117–1125.

[10] Heimerl J., Halder A., Benedict M.: *Experimental and computational investigation of a UAV-scale cycloidal rotor in forward flight*. In: Proc. The Vertical Flight Society's 77th Ann. Vertical Flight Society Forum and Technology Display, The Future of Vertical Flight, Virtual, May 10–14, 2021.

[11] Halder A., Benedict M.: *Nonlinear aeroelastic coupled trim analysis of a twin cyclocopter in forward flight*. AIAA J., 59, 2021, 305–319.

[12] Lee B., Saj V., Benedict M., Kalathil D.: *A Vision-Based Control Method for Autonomous Landing Of Vertical Flight Aircraft On A Moving Platform Without Using GPS*. In: Proc. The Vertical Flight Society's, 76th Ann. Forum and Technology Display, Virtual, Oct. 5–8, 2020.

[13] Denton H., Benedict M., Kang H., Hrishikeshavan V.: *Design, development and flight testing of a gun-launched rotary-wing micro air vehicle*. In: Proc. The Vertical Flight Society's, 76th Ann. Forum and Technology Display, Virtual, Oct. 5–8, 2020.

[14] Halder A., Benedict M.: *Understanding upward scalability of cycloidal rotors for large-scale UAS applications*. In: Proc. Aeromechanics for Advanced Vertical Flight Technical Meeting 2020, Transformative Vertical Flight 2020, San Jose, 21–23 Jan. 2020, 311–330.

[15] Runco C., Benedict M.: *Flight dynamics model identification of a meso-scale twin-cyclocopter in hover*. Paper presented at the 77th Ann. Vertical Flight Society Forum and Technology Display, The Future of Vertical Flight, Virtual, May 10-14, 2021.

[16] Runco C., Coleman D., Benedict M.: *Design and development of a 30 g cyclocopter*. J. Am. Helicopter Soc. **64**(2019), 1.

[17] Coleman D., Halder A., Saemi F., Runco C., Denton H., Lee B., Benedict M.: *Development of "Aria", a compact, ultra-quiet personal electric helicopter*. In: Proc. 77th Annual Vertical Flight Society Forum and Technology Display, FORUM 2021: The Future of Vertical Flight, Virtual, May 10–14, 2021.

[18] Koschorrek P., Siebert Ch., Haghani A., Jeinsch T.: *Dynamic positioning with active roll reduction using Voith Schneider propeller*. IFAC-PapersOnLine, **48**(2015), 16, 178–183.

[19] Schubert A., Koschorrek P., Kurowski M., Lampe B., Jeinsch T.: *Roll damping using Voith Schneider propeller a repetitive control approach*. IFAC-PapersOnLine **49**(2016), 23, 557–561.

[20] Hahn T., Koschorrek P., Jeinsch T.: *Parameter estimation of wave-induced oscillatory ship motion for wave filtering in dynamic positioning*. IFAC-PapersOnLine **51**(2018), 29, 183–188.

[21] Hashem I., Mohamed M.H.: *Aerodynamic performance enhancements of H-rotor Darrieus wind turbine*. Energy **142**(2018), 531–545

[22] Siegel S.: *Numerical benchmarking study of a cycloidal wave energy converter*. Renew. Energ. **134**(2019), 390–405.

[23] Siegel S.: *Wave radiation of a cycloidal wave energy converter*. Appl. Ocean Res. **49**(2015), 9–19.

[24] Bianchini A., Balduzzi F., Rainbird J., Peiro J., Graham M., Ferrara G.: *An experimental and numerical assessment of airfoil polars for use in Darrieus wind turbines – Part I: Flow curvature effects*. J. Eng. Gas Turb. Power **138**(2016), 032602-1.

[25] Dykas S., Majkut M., Smołka K., Strozik M., Chmielniak T., Staśko T.: *Numerical and experimental investigation of the fan with cycloidal rotor*. Mech. Mechanical Eng. **22**(2018), 2, 447–454.

[26] Staśko T., Dykas S., Majkut M., Smołka K.: An attempt to evaluate the cycloidal rotor fan performance, Open J. Fluid Dyn. 9(2019), 292–30.

[27] Shyy W., Lian Y., Tang J., Viieru D., Liu H.: *Aerodynamics of Low Reynolds Flyers*. Cambridge Univ. Press, 2008.

[28] *Ansys Fluent User Guide 2020 R1*. Ansys, Canonsburg 2020.

[29] Shrestha E., Yeo D., Benedict M., Chopra I.: *Development of a meso-scale cycloidal-rotor aircraft for micro air vehicle application*. Int. J. Micro Air Veh. **9**(2017), 3.

[30] Augusto J., Monteiro L., Pascoa J., Xisto C.: *Aerodynamic optimization of cyclorotors*. Aircraft Eng. Aerosp. Tec. **88**(2016), 2.